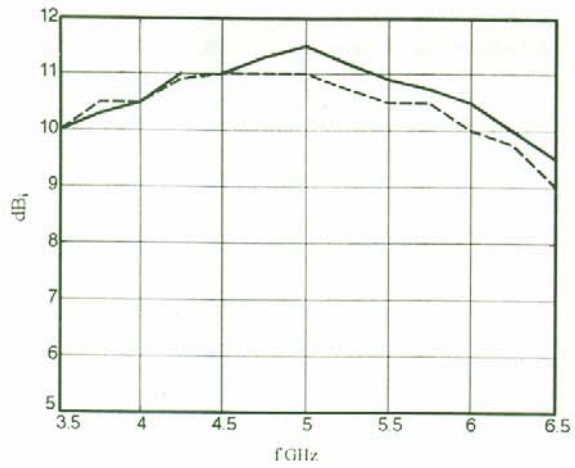

Figure 7 Available gain of V-slotted microstrip patch antennas: —— with parallel slots (antenna I); – – – – without parallel slots

were determined after extensive optimization, especially for antenna I, for low cross-polarization.

Typical radiation patterns at the low-frequency end are shown in Figures 5(a) and 5(b), which compare the E and H-plane patterns, and cross-polarization of the original V-slotted antenna and antenna I with vertical slots. The cross-polarization in the E-plane is negligible, but there is a beam-peak shift by as much as 10°. In the H-plane, there is some cross-polarization, and its peak is about −16 below the main beam. Radiation patterns at 6.5 GHz, well beyond the highest frequency for the impedance match, are shown in Figures 6(a) and 6(b). Significant copolar gain is still available, even with increased mismatch loss (Fig. 7). Thus, the copolar-gain bandwidth is even wider than the impedance bandwidth of the antenna. Figure 6(a) shows the increased cross-polarization of original V-slotted antenna and its significant reduction due to the edge slots. Figure 7 shows that by reducing the cross-polarization the radiated power has moved to the copular component. Consequently, at high frequencies the available gain has increased, even though the mismatch loss has been increasing with frequency beyond the antenna-impedance bandwidth.

CONCLUSION

It is shown that in a wideband microstrip antenna with a folded V-shaped slot, the relative peak cross-polarization increases almost exponentially with frequency, within the operating band. The introduction of two additional parallel slots at the patch edges, open at the upper edge, reduces this cross-polarization and makes it invariant with frequency. This suggests that, when placed at optimized locations, the parallel slots prevent the excitation of the higher-order modes at high frequencies and the antenna cross-polarization thus becomes nearly independent of frequency. Its magnitude is thus controlled by the antenna geometry, and remains low over a wide band.

REFERENCES

1. K.F. Lee, K.M. Luk, K.F. Tong, S.M. Shum, T. Huynh, and Q. Lee, Experimental and simulation studies of coaxially fed U-slot rectangular patch antenna, IEE Proc Microwaves Antennas Propagat 144 (1997), 354–358.
2. R. Bhalla and L. Shafai, Broadband patch antenna with a circular arc shaped slot, Proc IEEE Antennas Propagat Soc Int Symp, 2002, pp 394–397.
3. R. Bhalla and L. Shafai, Circular patch antenna with a circular arc slot and L-probe feeding, Proc ANTEM2002 Symp, Montreal, Canada, 2002, pp 459–462.
4. G.Z. Rafi and L. Shafai, V-slot microstrip antennas for wideband applications, Proc ANTEM2002 Symp, Montreal, Canada, 2002, pp 445–448.

MODELING OF PHOTONIC BAND GAP WAVEGUIDE COUPLERS

Yogita Nagpal and R.K. Sinha
Applied Physics Department
Delhi College of Engineering
Faculty of Technology, Delhi University
Bawana Road
Delhi–110 042, India

Received 8 March 2004

ABSTRACT: *The co-directional coupling between two photonic band gap (PBG) waveguides is studied. The designs of PBG waveguide couplers with different lattice arrangements are presented and their coupling characteristics are studied. Further, their application in the design of ultra-short optical multiplexer de-multiplexers (MUX-DEMUXs) has been investigated.* © 2004 Wiley Periodicals, Inc. Microwave Opt Technol Lett 43: 47–50, 2004; Published online in Wiley InterScience (www.interscience.wiley.com). DOI 10.1002/mop.20371

Key words: *integrated optics; photonic crystals (PhCs); waveguide couplers; multiplexer; de-multiplexer*

1. INTRODUCTION

Photonic crystals, microstructured materials in which the dielectric constant is periodically varied on length scale in one, two, or three directions with periodicity comparable to the wavelength of light, selectively transmit or reflect light at various wavelengths. A range of wavelengths in which a photonic crystal exhibits strong reflection is called a photonic band gap [1–8].

Photonic crystals (PhCs) or photonic band gap (PBG) materials are usually viewed as an optical analog of semiconductors that modify the properties of light similarly to a microscopic atomic lattice that creates a band gap for electrons in semiconductors. Hence, they provide a stimulating framework for the manipulation of light on a micrometer scale, as is required for the development of devices now envisaged for use in all optical networks. PhCs enable band engineering in photonics by which we can artificially control the optical properties of solids. Light can be guided in PBG structures by creating defects. Creating a linear defect in a PhC can make a PhC waveguide that allows directed light transmission for the frequencies inside the band gap. PBG waveguides have been a subject of interest because of their potential ability for tightly controlling the propagation of light with the possibility of the design and development of PBG-based directional couplers. Directional couplers are an essential component in the design of integrated optic devices for realizing all optical networks. When two waveguides are brought sufficiently close to each other so that their modal fields overlap, power can be transferred periodically between the two waveguides; such a structure is known as a directional coupler. Directional couplers have many interesting applications in power splitting, wavelength multiplexing/demultiplexing (MUX-DEMUX), polarization splitting, and so forth. Optical-communication systems that focus on dense WDM (DWDM)

systems employ wavelength division multiplexing/demultiplexing techniques and thus require compact components which provide accurate control of the wavelength to be used as wavelength-selective channel-dropping or channel-inserting filters. PBG-based waveguide couplers made of PBG materials offer exciting opportunities for designing compact wavelength-selective optical devices.

In the present paper, co-directional coupling between two closely placed PhC waveguides has been studied using the finite-difference time-domain (FDTD) method [9]. It is shown that changing the lattice arrangement in the PBG structure can alter the operational range of a PBG waveguide coupler. Thus, by altering the structural parameters as well as the lattice arrangement, it is possible to design and develop ultra-short optical devices in the same material system for desired wavelength windows. The spectral responses of PBG couplers with different lattice arrangements are investigated and it is shown that the coupling length of the PBG waveguide couplers falls in the micrometer regime, which is helpful in realizing compact optical devices. Further, the application of a PBG-directional coupler for the design of optical MUX-DEMUX has been discussed. The FDTD analyses of the proposed couplers show that significantly shorter optical MUX-DEMUXs can be designed using PBG waveguide couplers.

2. DESIGN OF CODIRECTIONAL PBG WAVEGUIDE COUPLERS

To design the PBG waveguide couplers we use two types of photonic crystals. The PBG1 is a square lattice of dielectric rods in air of radius $r = 0.18a$, where a is the lattice constant. The dielectric material has a dielectric constant of 10.5 (that is, refractive index $n = 3.24$, similar to the effective index in an InP/InGaAsP heterostructure system). The PBG2 is a triangular lattice of dielectric rods having $\varepsilon = 10.5$ of radius $r = 0.18a$ in air.

Both PBG1 and PBG2 yield PBGs for transverse-electric (TE) polarization, but no gap for transverse-magnetic (TM) polarization. Thus, only TE polarization has been considered. PBG1 has a band gap for TE polarization ranging from 0.324186 to 0.430233 in the normalized frequency frequency units (a/λ), where λ is the wavelength in a vacuum, calculated using the FDTD method. PBG2 exhibits a band gap for the TE mode ranging from 0.329767 to 0.480465 in the normalized frequency units. Figures 1 and 2 show the band diagrams for the PBG1 and PBG2 structures, respectively, obtained using the FDTD method. The light in the PBG1 and PBG2 structures can be guided by creating defects in them due to the photonic band gap (PBG) effect, if the frequency of the input light lies in the abovementioned band-gap regions.

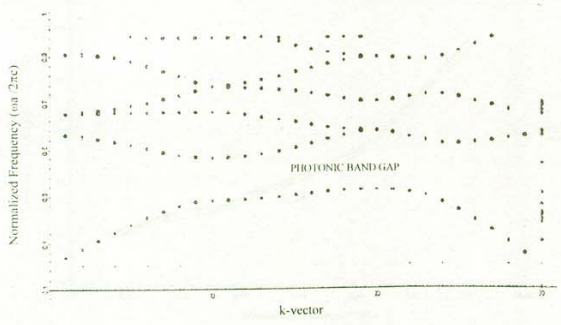

Figure 1 Band diagram for the PBG1 structure with a square-lattice arrangement of dielectric rods ($\varepsilon = 10.5$) in air

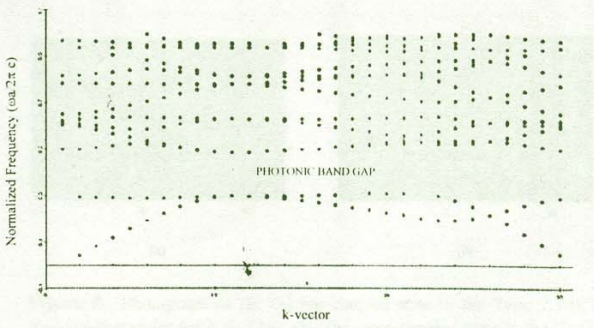

Figure 2 Band diagram for the PBG2 structure with a triangular-lattice arrangement of dielectric rods ($\varepsilon = 10.5$) in air

The waveguides in the PBG structures are obtained by creating linear defects in the PBG structures. To build the PBG waveguide couplers, two parallel waveguides are placed in close proximity to each other so that under suitable conditions the power can be transferred from one waveguide to another [10–19]. The two waveguides used to design PBG waveguide couplers are symmetric. These two parallel waveguides are separated by a row of dielectric rods air whose radius is $r_d \leq r$. Figure 3(a) depicts the proposed Type 1 PBG waveguide coupler, made by using the two PBG1 waveguides described above. Figure 3(b) depicts the proposed Type 2 waveguide coupler, which consists of two PBG2 waveguides.

3. NUMERICAL RESULTS

The FDTD calculations were done to study the coupling parameters of the proposed PBG waveguide couplers. The proposed PBG waveguide couplers were studied for TE polarization because for TM polarization, no band gap is observed for the constituent waveguides. The coupling length at various wavelengths for the proposed PBG waveguide couplers for TE polarization was calculated and the variation of the coupling length versus optical frequency was studied, which is necessary for the use of PBG waveguide couplers in various devices.

The coupling length L is given by

$$L = \frac{\pi}{\beta_e - \beta_o}, \tag{1}$$

where β_e is the propagation constant of even mode and β_o is the propagation constant of odd mode.

Figures 4 and 5 show the variation of normalized coupling length, obtained using the FDTD method, as a function of the

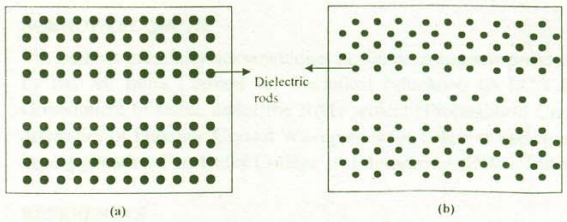

Figure 3 Schematic view of the proposed PBG waveguide coupler made from (a) two PBG1 waveguides (Type 1) and (b) two PBG2 waveguides (Type 2)

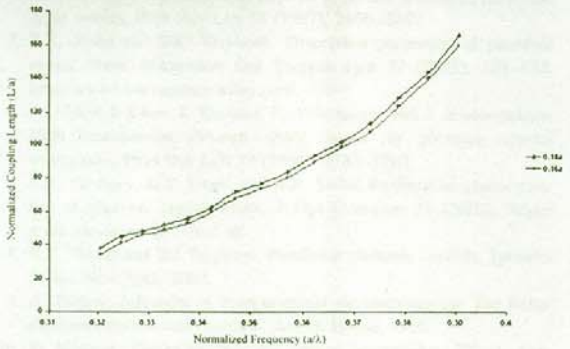

Figure 4 Normalized coupling length L/a as a function of normalized frequency a/λ for different r_d/a values for the TE mode for the proposed Type 1 PBG waveguide coupler

normalized frequency for two different values of normalized defect radius (r_d/a) for TE polarization for the proposed Type 1 and Type 2 PBG waveguide couplers, respectively.

The figures show that the Type 1 PBG waveguide coupler is functional for the TE mode in the range 0.324186 to 0.430233 and the Type 2 PBG waveguide coupler is functional for TE mode in the range 0.329767 to 0.480465 (in normalized frequency units). This is a direct consequence of the band-gap difference shown by the PBG structures. It is evident from the graphs that as r_d decreases, that is, as the barrier between the two waveguides decreases for each type, the coupling length decreases for the same frequency range, that is, $0.324186 \leq a/\lambda \leq 0.430233$ for the Type 1 PBG waveguide coupler and $0.329767 \leq a/\lambda \leq 0.480467$ for the Type 2 PBG waveguide coupler, for TE polarization. Thus, by changing the lattice arrangement, the operational frequency range of PBG waveguide couplers can be altered in a given material system.

Further, the graphs show that as a/λ decreases, the normalized coupling length L/a decreases. The coupling length decreases with an increase in wavelength. This can be explained by the fact that, as the wavelength is increased, the evanescent tail of the wave increases and it becomes easier for the wave to cross the barrier, thus leading to stronger coupling and hence smaller coupling length.

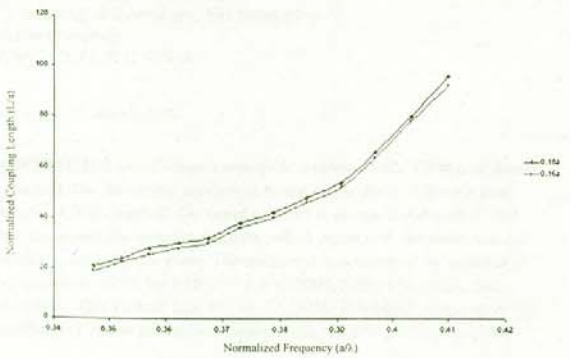

Figure 5 Normalized coupling length L/a as a function of normalized frequency a/λ for different r_d/a values for the TE mode for the proposed Type 2 PBG waveguide coupler

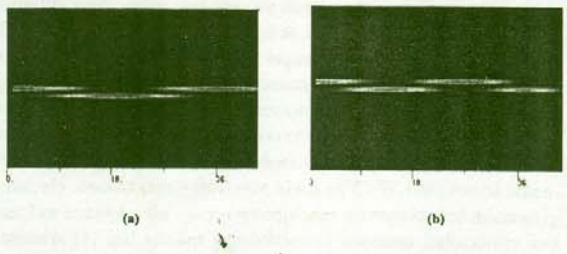

Figure 6 Photograph of the (a) bar-coupled state in the Type 2 PBG waveguide coupler for $\lambda = 1260$ nm; (b) cross-coupled state in the Type 2 PBG waveguide coupler for $\lambda = 1300$ nm

4. DESIGN OF PBG WAVEGUIDE MUX-DEMUX

Keeping in view the variation of coupling length shown by the PBG waveguide couplers with wavelength, the PBG waveguide coupler can separate two wavelengths λ_1 and λ_2, if it is in the bar-coupled state for one wavelength and cross-coupled state for the other wavelength. That is, after traversing the same distance in the PBG coupler, one wavelength λ_1 comes back to the original waveguide in which the light was launched (bar-coupled state) and the other wavelength λ_2 is in the adjacent waveguide (cross-coupled state). The photographs shown in Figures 6(a) and 6(b) exhibit bar-coupled state for $\lambda_1 = 1260$ nm and cross-coupled state for $\lambda_2 = 1300$ nm for the Type 2 PBG waveguide coupler used as an ultra-short optical MUX-DEMUX.

Thus, from the above analysis and the photographs (Fig. 6), it follows that the coupling length $L_{\lambda 1}$ at wavelength λ_1 and the coupling length $L_{\lambda 2}$ at wavelength λ_2 should satisfy the following relation to be used for the design of PBG-based MUX-DEMUX:

$$L_{\lambda 1}: L_{\lambda 2} = \text{even} : \text{odd}$$

$$L_{\lambda 1}: L_{\lambda 2} = \text{odd} : \text{even}. \qquad (2)$$

Thus, the use of PBG waveguide couplers can help in developing microscale optical integrated devices.

5. CONCLUSION

Two types of PBG waveguide couplers have been proposed and their wavelength responses have been studied. It has been shown that by changing the arrangement of dielectric rods, the operational range of PBG waveguide couplers can be tailored in a given material system. In addition, PBG waveguide couplers can be useful for making compact devices, as their coupling lengths have been shown to lie in the micrometer range. Further, the design of ultra-short PBG-based MUX-DEMUX has been proposed and will prove helpful in the miniaturization of optical integrated circuits.

ACKNOWLEDGMENT

The authors gratefully acknowledge the financial support provided by the All India Council for Technical Education (A.I.C.T.E), Government of India, under the R&D project "Propagation Characteristics of Photonic Crystal Waveguides for Telecom and Sensing Applications" at Delhi College of Engineering, Delhi, India.

REFERENCES

1. J.D. Joannopolous, R.D. Meade, and J.N. Winn, Photonic crystals: Molding the flow of light, Princeton University Press, Princeton, NJ, 1995.
2. K. Sakoda, Optical properties of photonic crystals, Springer Series, New York, 2001.

3. E. Yablonovitch, Inhibited spontaneous emission in solid state physics and electronics, Phys Rev Lett 58 (1987), 2059–2062.
4. S. John, Strong localization of photons in certain disordered dielectric super lattices, Phys Rev Lett 58 (1987), 2486–2489.
5. R.K. Sinha and S.K. Varshney, Dispersion properties of photonic crystal fibers, Microwave Opt Technol Lett 37 (2003), 129–132, http://www3.interscience.wiley.com.
6. A. Mekis, J. Chen, I. Kurland, P. Villeneuve, and J. Joannopolous, High transmission through sharp bends in photonic crystal waveguides, Phys Rev Lett 77 (1996), 3783–3790.
7. S.K. Varshney, M.P. Singh, and R.K. Sinha, Propagation characteristics of photonic crystal fibers, J Opt Commun 24 (2003), http://www.joc-online.de/online 46.
8. R.E. Slusher and B.J. Eggleton, Nonlinear photonic crystals, Springer Series, New York, 2002.
9. A. Taflove, Advances in computational electrodynamics: The finite-difference time-domain method, Artech House, 1998.
10. D. Marcuse, Theory of dielectric optical waveguides, 2nd ed, Academic Press, New York, 1991.
11. K. Okamoto, Fundamentals of optical waveguides, Academic Press, New York, 2000.
12. A.W. Snyder and J.D. Love, Optical waveguide theory, Chapman and Hall, New York, 1983.
13. M. Koshiba, Wavelength division multiplexing and demultiplexing with photonic crystal waveguide couplers, J Lightwave Technol 19 (2001), 1970–1975.
14. A. Martinez, F. Cuesta, and J. Marti, Ultra-short 2D photonic crystal directional couplers, Photonics Technol Lett 15 (2003), 69–696.
15. A. Sharkawy, S. Shi, and D.W. Prather, Electro-optical switching using coupled photonic crystal waveguides, Opt Express 10 (2002), 1048–1059.
16. A. Taflove, Advances in computational electrodynamics: The finite-difference time-domain method, Artech House, Boston, 1998.
17. A. Adibi, Y. Xu, R.K. Lee, and A. Yariv, Slab modes in photonic crystal optical waveguides, J Lightwave Technol 18 (2000), 1554–1564.
18. A. Adibi, R.K. Lee, Y. Xu, A. Yariv, and A. Scherer, Design of photonic crystal optical waveguides with single-mode propagation in the photonic band gap, Electron Lett 36 (2000), 1376–1377.
19. R. Costa, A. Melloni, and M. Martinelli, Band pass resonant filters in photonic crystal waveguides, Photon Technol Lett 15 (2003).

A NOVEL WIDEBAND COPLANAR-FED MONOPOLE ANTENNA

Wei Wang,[1] S. S. Zhong,[1] and Sheng-Bing Chen[2]
[1] School of Communication and Information Engineering
Shanghai University
Shanghai 200072, P.R. China
[2] Institute of Antennas and EM Scattering
Xidian University
Xi'an 710071, P.R. China

Received 27 March 2004

ABSTRACT: *A new T-shaped monopole antenna with a CPW feed line is presented. The theoretical analysis is based on the finite-difference time-domain (FDTD) method. The novel antenna is designed, fabricated, and then measured. The measured results, which agree with the numerical calculations very well, are given. The measured bandwidth of the antenna is approximately 116% for VSWR ≤ 2.0.* © 2004 Wiley Periodicals, Inc. Microwave Opt Technol Lett 43: 50–52, 2004; Published online in Wiley InterScience (www.interscience.wiley.com). DOI 10.1002/mop.20372

Key words: *monopole antenna; coplanar waveguide; bandwidth*

1. INTRODUCTION

Due to its low radiation losses, uniplanar nature, and high compatibility with active and passive devices, the coplanar waveguide (CPW) has been frequently used as an alternate to microstrip-line for feeding printed antennas, especially when used in MMIC applications. The microstrip antenna with a CPW feed also facilitates the integration of active devices and allows the realization of series as well as shunt connections on one side of the substrate, thus avoiding via-hole connections. Many investigators have extensively studied many different kinds of CPW-fed printed antennas. For example, the open-end coplanar waveguide fed microstrip antennas [1] and similar geometries of antennas inductively and capacitively coupled to coplanar lines [2] have been investigated experimentally. As one of the most widely used configurations, the CPW-fed slot antenna has been reported in [3–6] because of its well-matched performance.

In this paper, a new CPW-fed T-shaped monopole antenna is presented. The CPW feed-line and the T-shaped patch element are etched on the same side of a substrate. Its conductor ground is configurated as sloping with the monopole antenna instead of parallel to it. The impedance characteristics of the antenna are investigated by the FDTD method, which is widely used for analyzing antennas [7, 8]. The experimental results for the broadband impedance performance and the radiation patterns are presented. This antenna achieves optimal impedance characteristics with approximately 116% measured bandwidth for VSWR ≤ 2. The measured results show a good agreement with the simulation.

2. ANTENNA GEOMETRY AND CONCEPT

Figure 1 depicts the geometrical layout of the proposed CPW-fed T-shaped antenna. The T-shaped patch monopole is placed symmetrically on the centerline of the CPW line, at a distance t from the top side of the ground plane (which is modified in a slope shape), where L_m and W_m are the length and width of the patch monopole, respectively, D_{max} is the bottom width of the ground plane, and D_{min} is the width of the top side. The CPW feed line has 50Ω characteristic impedance. As shown in Figure 1, the monopole element and ground plane are etched on the same side of the substrate, while the other side is without any metallization.

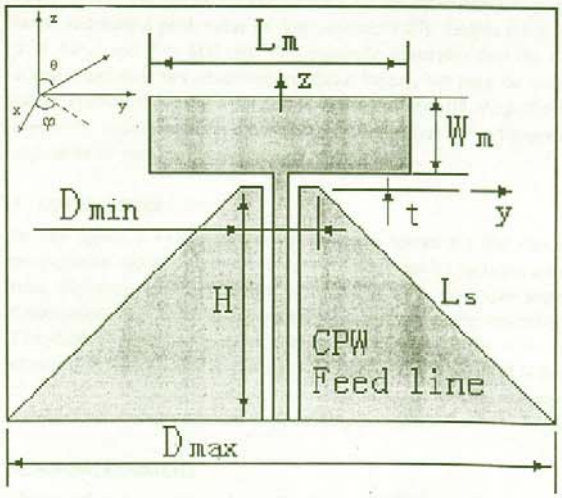

Figure 1 Configuration of the proposed antenna

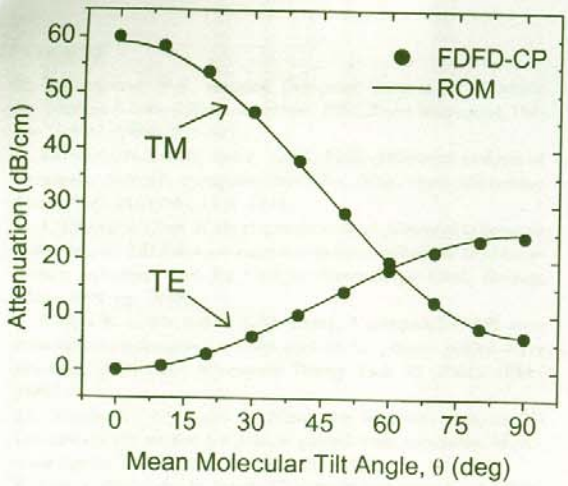

Figure 5 Attenuation of the lowest-order TE and TM modes of the multilayered waveguide depicted in Fig. 4. Very close correlation is observed between the FDFD-CP method (dots) and the results obtained using the ray optics model (ROM), described in [14]

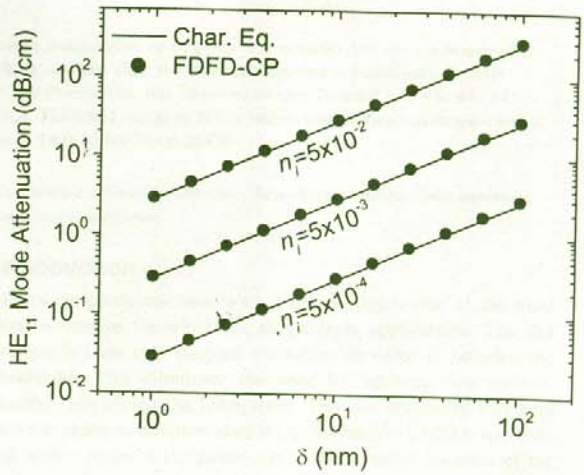

Figure 7 Attenuation of the lowest-order (HE_{11}) mode of the optical fiber shown in Fig. 6. The results obtained using the FDFD-CP method (dots) are compared to the solution of the characteristic equation for the weakly guiding approximation, given in [16]. Results are shown for three different values of n_i, the imaginary portion of the refractive index of the thin inner cladding layer

method, as compared to the results obtained using the ROM. The results match very closely across the entire range of tilt angles, thus demonstrating that the FDFD-CP method properly accounts for anisotropy in the thin, lossy layer.

3.3. Optical Fiber with Thin, Lossy Inner Cladding

To demonstrate the applicability of the FDFD-CP method to nonplanar structures, it was applied to the optical fiber shown in Figure 6. The index of the cladding, $n_o = 1.44402$, is obtained from the Sellmeier equation for fused silica [15] at $\lambda = 1550$ nm. The core/cladding index difference Δn is assumed to be 0.0045, and the core radius a is 4.15 μm. The complex index of refraction of the thin inner-cladding layer is given by $n_o - jn_i$. If $n_i \ll n_o$, the weakly guiding approximation is valid and the scalar wave

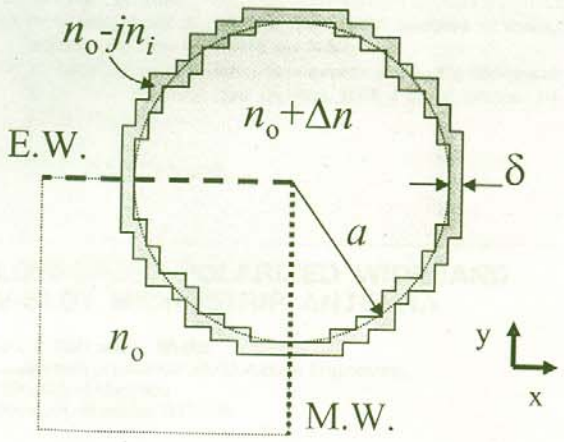

Figure 6 Optical fiber, with thin lossy layer of thickness δ inserted between the core and cladding. The circular thin layer was approximated using orthogonal segments. The symmetry of the structure was exploited to reduce computational time by inserting electric and magnetic symmetry walls (E.W. and M.W.) and only considering the lower left quadrant of the structure (parameter values are given in the text)

equation may be used to obtain the characteristic equation for the structure, as in [16]. The characteristic equation is then iteratively solved for the complex propagation constants of the guided modes. For the FDFD-CP method, the thin inner-cladding layer was approximated by a combination of continuously joined orthogonal segments, as illustrated in Figure 6. In addition, electric and magnetic symmetry walls were placed as shown in the figure in order to reduce computational time.

Figure 7 shows the calculated attenuation of the fundamental HE_{11} fiber mode for $n_i = 5 \times 10^{-2}$, 5×10^{-3}, and 5×10^{-4}. The values obtained using the FDFD-CP method correlate well with those obtained from the characteristic equation. The effective index n_{eff} is not shown, but was found to be minimally affected by the presence of the lossy layer. For example, for $n_i = 5 \times 10^{-2}$, the variation of n_{eff} was less than 0.01% over the range of δ shown in the figure. The predicted attenuation, on the other hand, is quite large, reaching a peak value of approximately 270 dB/cm for $n_i = 5 \times 10^{-2}$ and $\delta = 100$ nm. This example illustrates that the CP approximation is not restricted to planar layers, but may be accurately applied to waveguides incorporating arbitrarily shaped thin layers by approximating the layer as a collection of orthogonal segments of varying length and/or width.

4. CONCLUSION

In this paper, a FDFD method to directly solves for the modal propagation and attenuation constants of waveguides incorporating thin, dielectric, or lossy layers while retaining a grid size many times larger than the thickness of the thin layer has been described. The method was shown to be applicable to planar and nonplanar structures. The primary advantage of this FDFD-CP method is that it can be accurately applied to waveguides of arbitrary cross section and is not restricted to specific geometries.

ACKNOWLEDGMENT

This work was supported by the National Science Foundation under grant no. ECS-245716.

REFERENCES

1. E. Schweig and W.B. Bridges, Computer analysis of dielectric waveguides: A finite-difference method, IEEE Trans Microwave Theory Tech 32 (1984), 531–541.
2. K. Bierworth, N. Schulz, and F. Arndt, Finite-difference analysis of rectangular dielectric waveguide structures, IEEE Trans Microwave Theory Tech 34 (1986), 1104–1114.
3. M.-L. Liu and Z. Chen, A direct computation of propagation constant using compact 2-D full-wave eigen-based finite-difference frequency-domain technique, Proc Int Comput Electromagn Conf, Beijing, China, 1999, pp. 78–81.
4. Y.-J. Zhao, K.-L. Wu, and K.-K.M. Cheng, A compact 2-D full-wave finite-difference frequency-domain method for general guided wave structures, IEEE Trans Microwave Theory Tech 50 (2002), 1844–1848.
5. J.A. Perede, A. Vega, and A. Prieto, An improved compact 2D full-wave FDFD method for general guided wave structures, Microwave Optical Technol Lett 38 (2003), 331–335.
6. R. Lotz, J. Ritter, and F. Arndt, 3D subgrid technique for the finite difference method in the frequency domain, 1998 Int Microwave Symp Dig 3 (1998), 1739–1742.
7. L. Kulas and M. Mrozowski, Reduced order models of refined Yee's cells, IEEE Microwave Wireless Compon Lett 13 (2003), 164–166.
8. A. Taflove, K.R. Umashankar, B. Beker, F. Harfoush, and K.S. Yee, Detailed FD-TD analysis of electromagnetic fields penetrating narrow slots and lapped joints in thick conducting screens, IEEE Trans Antennas Propagat 36 (1988), 247–257.
9. J.G. Maloney and G.S. Smith, The efficient modeling of thin material layers in the finite-difference time-domain (FDTD) method, IEEE Trans Antennas Propagat 40 (1992), 323–330.
10. K.S. Yee, Numerical solution of initial boundary value problems involving Maxwell's equations in isotropic media, IEEE Trans Antennas Propagat 14 (1966), 302–307.
11. A. Taflove, Computational electrodynamics: The finite-difference time-domain method, Artech House, Boston, 1995.
12. The MathWorks, Inc., 3 Apple Hill Drive, Natick, MA 01760-2098.
13. R.B. Lehoucq, D.C. Sorensen, and C. Yang, ARPACK users' guide: Solution of large-scale eigenvalue problems with implicitly restarted Arnoldi methods, 1998, http://www.caam.rice.edu/software/ARPACK.
14. S.B. Mendes and S.S. Saavedra, Comparative analysis of absorbance calculations for integrated optical waveguide configurations by use of the ray optics model and the electromagnetic wave theory, Appl Optics 39 (2000), 612–621.
15. W.G. Driscoll and W. Vaughan (Eds.), OSA handbook of optics, McGraw-Hill, New York, 1978, pp. 7–85.
16. S. Kawakami and S. Nishida, Characteristics of a double clad optical fiber with a low-index inner cladding, IEEE J Quant Electron 10 (1974), 879–887.

LOW-CROSS-POLARIZED WIDEBAND V-SLOT MICROSTRIP ANTENNA

Gh. Z. Rafi and L. Shafai
Department of Electrical and Computer Engineering
University of Manitoba
Winnipeg, Manitoba, R3T 5V6

Received 9 March 2004

ABSTRACT: *The performance of a V-slotted microstrip patch antenna, with and without additional edge slots, is investigated. It is shown that the V-slotted patch is broadband, but its cross polarization increases with frequency. Placing two additional rectangular slots at the patch edges, parallel to its shorter side, eliminates the problem without affecting the bandwidth. The cross-polarization becomes independent of frequency. It remains low over a bandwidth, which is wider than the antenna-impedance bandwidth.* © 2004 Wiley Periodicals, Inc. Microwave Opt Technol Lett 43: 44–47, 2004; Published online in Wiley InterScience (www.interscience.wiley.com). DOI 10.1002/mop.20370

Key words: *microstrip antennas; broadband antennas; slot antennas; low cross polarization*

INTRODUCTION

Microstrip patch antennas with a folded slot is one of the most popular designs for wideband, single-layer applications. The slot and patch form two coupled resonators in order to broaden the bandwidth. This eliminates the need for stacking two patches, thereby simplifying the fabrication. The slot originally was bent into a U shape to accommodate it on the patch [1], which was then fed with a probe at the patch center. This central location of the probe and the symmetry of the patch and slot eliminated the first mode. The resultant antenna then operated in the second mode, with the patch currents running parallel to its shorter edge. Impedance bandwidths as high as 30% for a probe-fed patch were obtained for the U-slotted patch [1]. In [2], a circular-arc slot over a rectangular patch was used to enhance its bandwidth to about 30%, which is similar to that of a U-slot. Larger bandwidths were also obtained by other slots. In [3], a bent dipole was used to feed the same circular-arc slot, but on a circular-patch microstrip antenna. The bandwidth was increased to about 40%, but because of the bent probe shape, the configuration was more complex. These studies confirmed the similarity of rectangular and circular microstrip patches in the bandwidth performance, as well as the similarity of the U- and circular-arc-shaped slots on them. Recently, it was shown that by modifying the slot shape from a U to a truncated V, the angle of the V arm can be used as an additional parameter to further increase the impedance bandwidth to 36.5% [4]. The geometry of this antenna is shown in Figure 1. One area of difficulty with both U and V slotted antennas is the cross polarization. Cutting the U or V slot on the patch forces the patch currents to bend around the slot. Consequently, the patch current has an orthogonal component that contributes to cross-polar radiation. Because of the central location of the probe and the symmetry of both slot and patch geometries, the generated cross-polarized current is in the same direction as the currents of the next-higher-order mode of the patch in the horizontal W direction. Thus, their similarity aids in the excitation of this higher mode. As a result, the cross polarization of the radiated field in the H-plane, that is, the horizontal plane in Figure 1, increases with frequency. In this paper, we investigate the influence of additional slots on the radiation properties of the slotted wideband microstrip antennas, such as gain and cross-polarization.

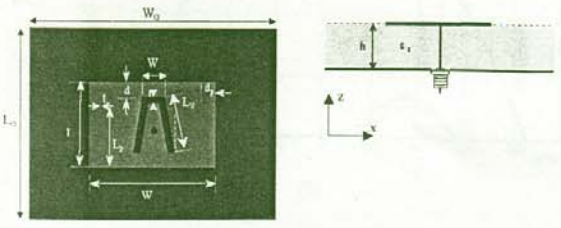

Figure 1 Geometry of the wideband V-slotted microstrip patch antenna: $L_G = W_G = 60$ mm, $h = 5.5$ mm, $\varepsilon_r = 1.05$, $L = 26$ mm, $W = 36$ mm, $\theta = 10°$, $L_V = 20.7$ mm, $W_V = 8.8$ mm, $t = 2$ mm, $d = 2.3$ mm

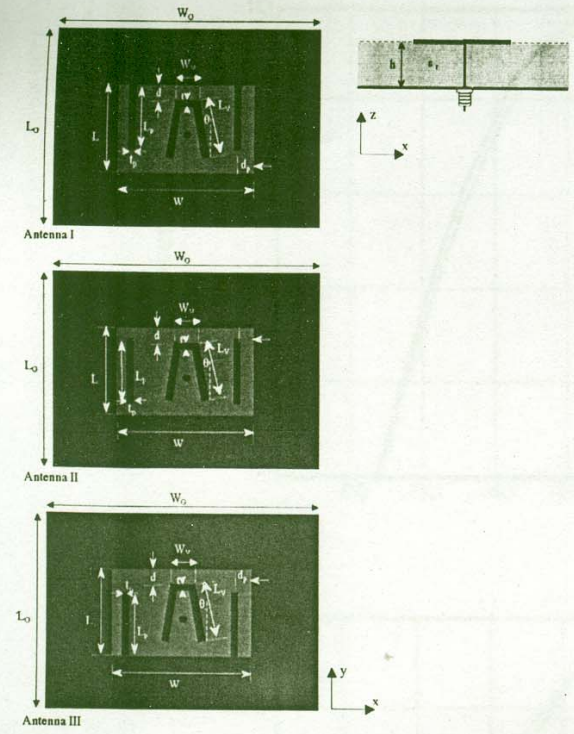

Figure 2 Geometries of wideband V-slotted microstrip patch antennas with two parallel-edge slots of different configurations: L_p = 22 mm, t_p = 1.5 mm, d_p = 3 mm

SLOTTED PATCH WITH EDGE SLOTS

All wideband slotted patches, regardless of the slot shape, seem to have similar polarization performance. The cross-polarization of the radiated field increases with frequency. This is due to the enhanced excitation of the second mode along the longer W dimension of the rectangular patch, which is caused by bending the

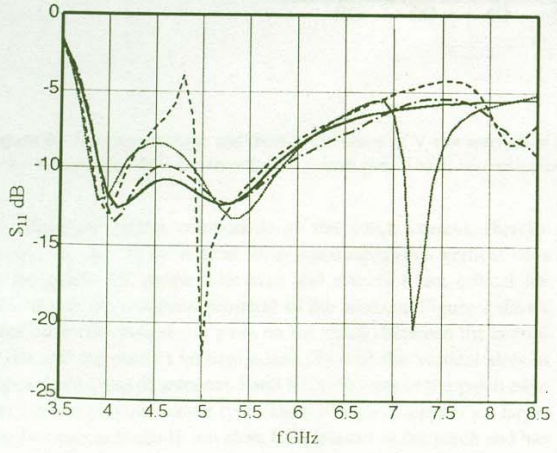

Figure 3 Return losses for the V-slot microstrip patch antennas of Figs. 1 and 2: – · – · – without parallel slots; —— with two parallel edge slots open at the top (antenna I); ------ with two parallel edge slots at the middle (antenna II); ····· with two parallel edge slots open at the bottom (antenna III)

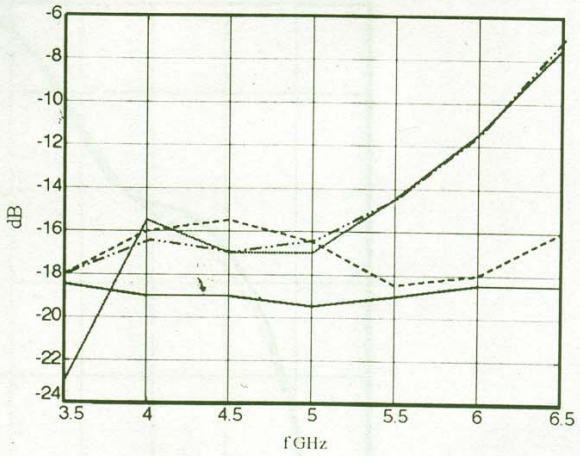

Figure 4 Cross-polarization levels in H-plane vs. frequency for different V-slot antennas of Fig. 3: – · – · – without parallel slots; —— with two parallel edge slots open at the top (antenna I); ------ with two parallel edge slots at the middle (antenna II); ····· with two parallel edge slots open at the bottom (antenna III)

patch currents around the slots. This mode is horizontally polarized (see Fig. 1), which indicates it is orthogonal to the wideband vertical mode and contributes to cross polarization. A possible way

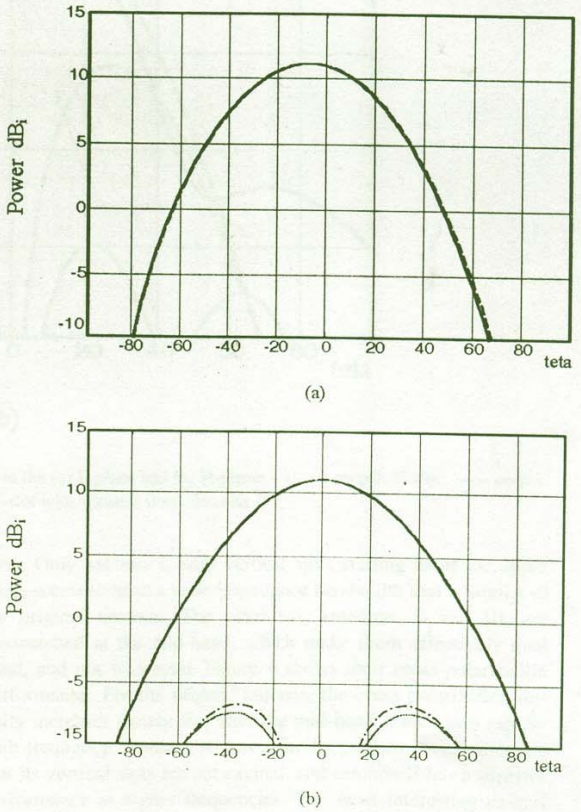

Figure 5 Radiation patterns and cross-polarization of V-slot antennas at 4 GHz in the (a) E-plane and (b) H-plane: – · – · – co-pol. V-slot; —— co-pol. V-slot with parallel slots (antenna I); ------ cross-pol. V-slot; ····· cross-pol. V-slot with parallel slots (antenna I)

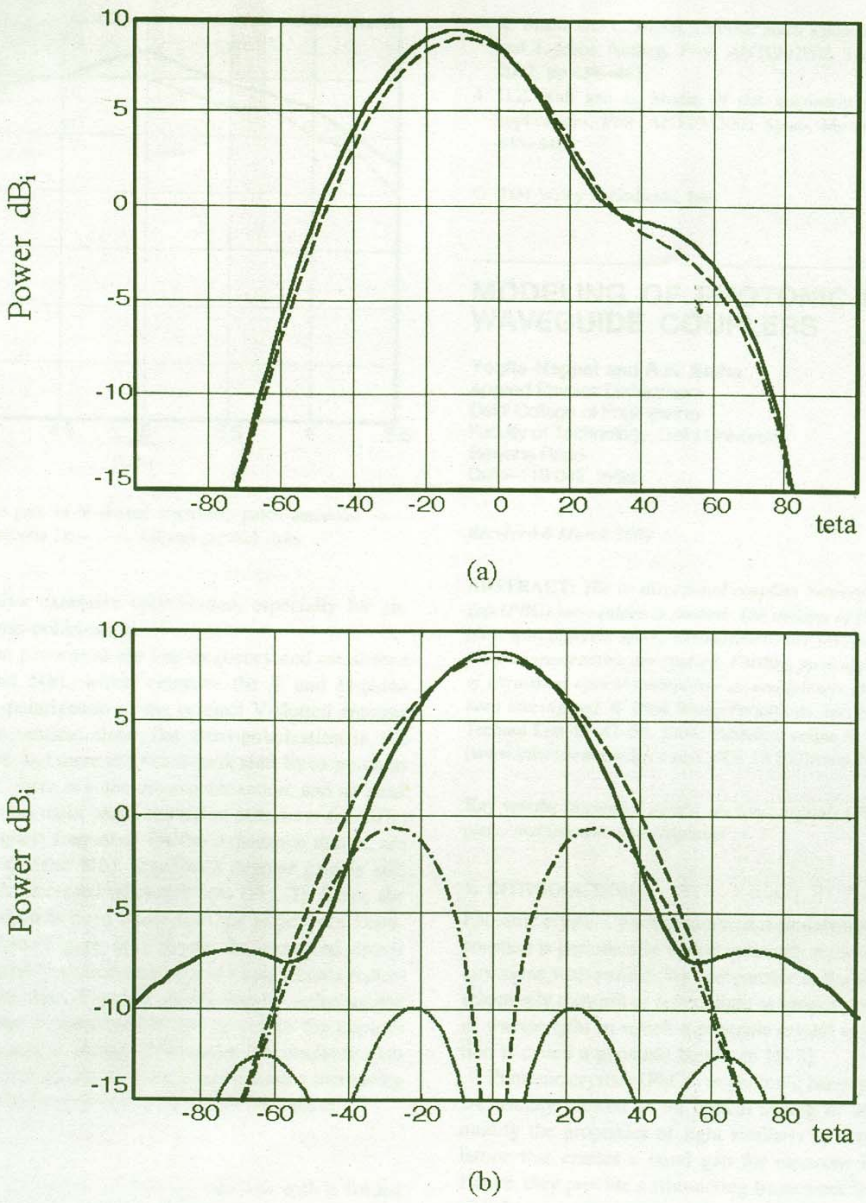

Figure 6 Radiation patterns and cross-polarization of V-slot antennas at 6.5 GHz in the (a) E-plane and (b) H-plane: – · – · – co-pol. V-slot; —— co-pol. V-slot with parallel slots (antenna I); ------ cross-pol. V-slot; ····· cross-pol. V-slot with parallel slots (antenna I)

to reduce the lateral component of the patch current, thereby forcing the slots to be vertical, is to place additional vertical slots on the patch. Of course, slot size and direction are critical for maintaining the wideband property of the antenna. Figure 2 shows three different vertical-slot pairs on the patch, between the central V slot and the patch's vertical edges. Two of the vertical slots in Figure 2, designated antennas I and III, terminate at the patch edge and therefore are monopole type. Their electrical lengths are large. The last one, antenna II, has slots fully placed in the patch and has a shorter electrical length. The antennas' performance for bandwidth and radiation characteristics were investigated in detail and compared.

Figure 3 shows the computed return loss of these antennas along with that of the original V-slotted patch, without the vertical slots. Only antenna I, with vertical slots starting from the upper edge, seems to have a wide-impedance bandwidth that is similar to the original antenna. The other two antennas, II and III, are mismatched at the mid-hand, which make them effectively dual band, and not wideband. Figure 4 shows their cross-polarization performance. For the original antenna, the cross polarization initially increases slowly, but after the mid-band it increases rapidly with frequency. Antenna III has a similar performance, indicating that its vertical slots are not excited, and antenna II has a superior performance at higher frequencies. The most interesting case is antenna I, for which the cross polarization remains constant, even beyond its upper-impedance match frequency, for $S_{11} = -10$ dB. In other words, its cross polarization is independent of frequency. Note that these properties and the vertical-slot size and location